Macromolecules

Article

pubs.acs.org/Macromolecules

Mechanochemical Route to Graphene-Supported Iron Catalysts for Olefin Polymerization and in Situ Formation of Carbon/Polyolefin Nanocomposites

F. Beckert,[†,‡,§] S. Bodendorfer,[†,‡,§] W. Zhang,[†] R. Thomann,[‡] and R. Mülhaupt*[,†,‡]

[†]Institute for Macromolecular Chemistry, Albert-Ludwigs-University of Freiburg, Stefan-Meier-Straße 31, D-79104 Freiburg, Germany

[‡]Freiburg Materials Research Center FMF, Stefan-Meier-Straße 21, D-79104 Freiburg, Germany

ABSTRACT: A facile one-step mechanochemical process converts graphite into highly active graphene-supported iron catalysts for ethylene polymerization and the in situ formation of graphene/polyethylene nanocomposites. Key feature is the dry grinding of graphite in a steel ball mill under carbon dioxide pressure, affording high surface area edge-carboxylated graphene accompanied by simultaneous immobilization of Fe^{2+}, formed by iron abrasion and electron transfer reaction. In contrast, as evidenced by Mössbauer spectroscopy, grinding graphite in the absence of carbon dioxide under nitrogen or argon pressure produces predominantly Fe^{0} together with Fe^{3+} supported on nitrogen-functionalized graphene or micronized graphite, respectively. On addition of bisiminopyridine (BIP) and activation with methylaluminoxane (MAO), only the Fe^{2+} catalyst supported on edge-functionalized graphene (Fe@MG-CO_2) polymerizes ethylene in high yields, producing polyethylene with a molar mass of 180 kg/mol and a polydispersity of 6.1. According to the transmission electron microscopic analysis of polyethylene morphology, functionalized graphene with low aspect ratio is uniformly dispersed in the polyethylene matrix. Hence, this mechanochemical catalyst preparation enables the fabrication of graphene/polyolefin nanocomposites with high carbon content by polymerization filling using cost-effective graphite as raw material without requiring tedious and expensive graphite functionalization in separate steps.

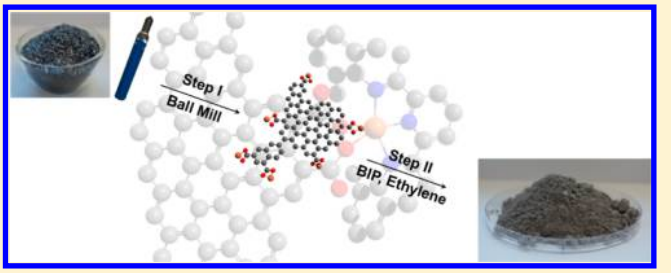

INTRODUCTION

During the past decade, the development of graphene and graphene-based polymeric composite materials is attracting considerable attention in academia and industry, stimulated by the pioneering advances of Geim and Novoselov.[1] As a single carbon layer of the graphite lattice and two-dimensional carbon macromolecule, graphene exhibits ultrahigh modulus,[2] optical transparency combined with electrical conductivity[3] and a large specific surface area,[4] which enables the immobilization of metal nanoparticles and the use as support material for manifold reactions.[5−8] However, the availability of defect-free graphene is still limited, owing to its expensive synthesis such as chemical vapor deposition (CVD)[9,10] or epitaxial growth.[11] In a more cost-effective preparation, functionalized graphene (FG) is produced by the oxidation of graphite followed by chemical[12] or thermal[13] reduction. By tuning the reaction parameters, FG materials are tailored regarding their functional group density, oxygen content as well as the surface area and the electrical properties. However, graphite intercalation, oxidation and subsequent reduction requires the use of strong acids,[14,15] hazardous oxidizing agents and frequently also toxic reducing agents such as hydrazine.[16,17] In a much more cost- and time-efficient route, mechanochemical synthesis has been introduced in order to achieve both mechanical delamination and functionalization in a facile one-step grinding process. The wet grinding process employs liquid media with matched polarity,[18−20] frequently assisted by the addition of surfactants such as SDS[18] or melamine.[21] In a dry grinding process, Jeon et al.[22] reported on the mechanochemical formation of edge-carboxylated graphene produced by ball milling of graphite together with dry ice. According to their hypothesis, the in situ formed dangling bonds react with CO_2 and incorporate carboxylic acid groups allocated exclusively at the graphene edges. This is in contrast to functionalized graphene produced from graphite oxide, which decomposes to form nanoporous graphene with much higher content of structural defects. In a recent advance, the same group published the direct mechanochemical nitrogen fixation by ball-milling of graphite under N_2 atmosphere.[23] In all mechanochemical syntheses, metal impurities originating from steel abrasion must be removed in a further step, using either magnetic forces[24] or washing with hydrochloric acid.[25] No attempts have been made to exploit the mechanical immobilization of iron complexes and nanoparticles produced by abrasion during dry grinding. Iron catalysts are attractive in numerous reactions, including growth of carbon nanotubes,[26] direct C−H transformation,[27] Fischer−

Received: August 5, 2014
Revised: September 24, 2014

   dx.doi.org/10.1021/ma501602j | *Macromolecules* XXXX, XXX, XXX−XXX

Tropsch synthesis,[28] and epoxidation of alkenes[29] as well as ethylene polymerization.[30]

Herein we report on the facile mechanochemical synthesis of a highly active iron ethylene polymerization catalysts supported on edge-carboxylated graphene. This dry grinding process exploits graphite as raw material. Whereas most immobilization strategies require several steps to immobilize iron on functionalized graphene and other support materials,[31−33] this mechanochemical approach combines formation of edge-carboxylated graphene support and in situ immobilization of iron in a single step without requiring either solvent addition or other chemical functionalization. Furthermore, we exploit this mechanical process for producing in situ carbon/polyolefin nanocomposites by polymerization filling technique.

EXPERIMENTAL SECTION

Materials. Natural graphite (KFL 99.5 from AMG Mining former Kropfmühl) was dried at 60 °C under vacuum (10 mbar) for 48 h prior to use. CO_2, N_2, and argon were received from Air Liquide and used without further purification. All polymerization reactions were carried out under dry argon atmosphere using standard Schlenk techniques and a glovebox. Toluene (anhydrous) and *n*-heptane (anhydrous) were purchased from Sigma-Aldrich. The solvents were purified using a Vacuum Atmospheres Co. solvent purifier. MAO, purchased from Crompton, with Al content of 10 wt % in toluene was stored under argon atmosphere. Ethylene was purchased from Air Liquide and was used without any further purification.

One milling reactor was custom-made of stainless steel (1.4301 − X2CrNi18−10; V = 370 cm^3), whereas the zirconia reactor (V = 1150 cm^3) was received from Retsch and equipped with a custom-made lid. Preferably, the balls (50 pieces) and the mill were made of the same materials. The samples were milled using a planetary ball mill PM 100 from Retsch.

Synthesis of MG-X (Typical Procedure). Graphite (5.0 g) was added to a dried mill chamber (48 h at 60 °C, 10 mbar) and evacuated (0.1 mbar) for 15 min. Afterward the milling reactor was pressurized with CO_2, N_2, or Argon (7 bar) and milling was performed at 250 rpm for the duration of 48 or 96 h. Specific samples were stored under inert argon atmosphere, since exposure to air was accompanied by violent sparkling and formation of red glowing embers.

Synthesis of the Bisiminopyridine Ligand (BIP). 2,6-Diacetylpyridine (5.0 g, 31 mmol) and 2,6-dimethyaniline (8.1 mL, 65 mmol) were suspended in toluene (100 mL). A catalytic amount of *p*-toluenesulfonic acid was added to the suspension. The reaction mixture was stirred at 140 °C for 2 h with adapted water separator. Afterward the solvent was removed at reduced pressure, the solid residue was recrystallized from ethyl acetate (2 × 2 mL), and washed with methanol (3 × 5 mL). The product was diluted in benzene and extracted by freeze-drying.

^{1}H NMR (300 MHz, $CDCl_3$/TMS): δ = 2.05 (s, 1′-H_3, 2′-H_3), 2.24 (s, 3′-H_3), 6.94 (dd, $J_{12-11} = J_{12-13}$ = 7.5, 12-H), 7.08 (d, $J_{11-12} = J_{13-12}$ = 7.6, 11-H, 13-H), 7.91 (dd, $J_{4,3} = J_{4,5}$ = 7.4, 4-H), 8.48 (d, $J_{4,3} = J_{4,5}$ = 7.4, 3-H, 5-H).

Ethylene Polymerization. Reactions were carried out in a 600 mL Büchi stainless steel autoclave equipped with a mechanical stirrer and a software interface to analyze polymerization kinetics.

The MG-X support was preheated at 40 °C for 1 h. Then it was dispersed in toluene (20 mL) and sonicated for 10 min. The bisiminopyridine ligand (BIP) was dissolved in toluene (10 mL) and added to the MG-X dispersion, followed by sonication for 60 min. After the addition of MAO, the mixture was stirred for 5 min and sonicated for further 10 min. The activated dispersion was washed with fresh toluene to remove excess of MAO and BIP. The reactor was charged with *n*-heptane (567 mL) and 50% of the needed MAO amount as scavenger. During the polymerization the temperature was kept at 40 °C with an ethylene pressure of 5 bar and a polymerization time of 120 min while applying a stirring speed of 400 s^{-1}. The reaction was quenched by venting the vessel. The reaction mixture was precipitated in methanol (600 mL) with BHT (0.01 wt %) as stabilizer. The polymer was filtered and dried in vacuum (10^{-2} mbar) at 60 °C for 6 h. Table 1 summarizes the experimental conditions of Fe-catalyzed polymerizations.

Table 1. Experimental Conditions of the Fe-Catalyzed Ethylene Polymerizations

	m(MG-X) [mg]	n(Fe)[a] [μmol]/[wt %]	n(BIP) [μmol]	Al:Fe [mol/mol]
FeBIP	–	4.47	4.47	100:1
Fe@MG-N_2-Ar	250	44.7/1	44.7	100:1
Fe@MG-CO_2-atm	250	178/4	200	100:1
Fe@MG-CO_2-Ar	250	44.6/1	44.7	100:1

[a]Determined by EDX measurements.

Instrumentation. Transmission electron microscopy (TEM) was performed using a Zeiss/LEO 912 W at 120 kV. The samples were cryo-microtomed or directly collected from dispersions on Cu grids. Scanning electron microscopy (SEM) images were obtained with a Quanta 250 FEG from FEI using backscattered mode. The accelerating voltage was set to 20 kV. Atomic force microscopy (AFM) measurements were performed on MultiMode AFM with a Nanoscope IIIa controller (Veeco DI Instruments), using tapping mode and Si cantilevers of supersharp type with about 2−10 nm radius of curvature and 160 kHz resonance frequency. FT-IR spectra were measured, using KBr specimen containing the sample. With a Vektor 22 from Bruker 32 scans with a resolution of 2 cm^{-1} were recorded. As background the spectrum of a pristine KBr disc was used. The C, H, and N ratio was determined using elemental analysis with a VarioEL from Elementaranalysensysteme GmbH. The Fe, O, and Zr ratio was determined with energy-dispersive X-ray spectroscopy (EDX) using an Inca x-act from Oxford Instruments operating at 20 kV. Mössbauer spectra were recorded with a ^{57}Co source in a Rh matrix using an alternating acceleration Wissel Mössbauer spectrometer operated in the transmission mode and was equipped with a Janis closed-cycle helium cryostat. Isomer shifts were recorded relative to iron metal at ambient temperature.

Molecular weight determination was performed with a PL-200 chromatograph (Polymer Laboratories) using differential refractive index (DRI). Measurements were performed at 150 °C with three PLGel Olexis columns, calibrated with 12 polystyrene samples with a narrow molecular weight distribution. 1,2,4-Trichlorobenzene (Merck) was used as solvent, stabilized with 2,6-di-*tert*-butyl-(4-methylphenol) (0.2 wt %, Aldrich). A flow rate of 1.0 mL/min was used. Thermal properties were determined with differential scanning calorimetry (DSC) using a Pyris 1 (PerkinElmer). The samples were heated from room temperature to 260 °C with a heating rate of 20 K/min. Then cycles were performed using a heating rate of 10 and 5 K/min. For analysis of crystallization behavior a heating rate of 10 K/min was used.

Polymers were stabilized using 0.5 wt % of a Irgafos 168/Irganox 1010 (1/4) blend. Melt compounding was performed using a DSM twin screw micro compounder (XPlore) at 190 °C for 2 min. Specimens were prepared by DSM micro injection molding (XPlore) at 190 °C. Young's modulus and elongation at break were measured by stress−strain test (Zwick Z005) according to EN ISO 527−2. Results are the average out of three measurements.

RESULTS

Pioneered by Brookhart et al., the methylalumoxane (MAO) activation of bisiminopyridine iron complexes is well-known to afford highly active single-site catalysts for olefin polymerization.[34] Such catalysts systems were immobilized on various nanofillers in order to produce in situ nanocomposites with

dx.doi.org/10.1021/ma501602j | Macromolecules XXXX, XXX, XXX−XXX

uniform dispersion of the nanofiller in the polyolefin matrix.[35] This in situ dispersion during polymerization, named polymerization filling technique by Dubois, takes place in gas phase or diluents with low viscosity. This is advantageous with respect to melt compounding, since nanofillers are rather difficult to disperse in highly viscous polymer melts. In the case of carbon/polyolefin nanocomposites the high aspect ratio of carbon nanofillers plays an important role with respect to achieving matrix reinforcement and low percolation threshold, as reflected by high electrical conductivity at low carbon content.[36,37] While micronized graphite with high carbon content, mostly consisting of particles >10 μm, is extensively used as filler since many years, little is known concerning the use of graphene produced by mechanochemical processes. During recent years, Jeon et al. introduced a very versatile mechanochemical process for preparing edge-functionalized graphene. They reported on dry ball milling of graphite in the presence of dry ice in order to produce edge-selective carboxylated graphene in a process which is suitable for scale-up.[22] Moreover, ball milling under nitrogen enables the incorporation of nitrogen into graphene. XPS studies revealed the presence of C−N and N−N, thus Jeon et al. proposed the formation of 5- and 6-membered rings at the edges of the graphene platelets.[23] In contrast, milling under argon atmosphere under identical conditions fails to incorporate functional groups in the absence of oxygen. In the presence of air, the resulting nanometer-scaled carbon is readily oxidized. Typically, iron nanoparticles, resulting from steel abrasion, are removed by washing with HCl. Here, we exploit steel abrasion to prepare iron catalysts supported on carboxylated and nitrogenated graphene, produced by grinding graphite in a planetary ball mill under carbon dioxide or nitrogen pressure, respectively. Hence, the simultaneous delamination of graphite and immobilization of iron by steel abrasion is achieved. Instead of adding dry ice, which contains water traces, we pressurized the ball mill with carbon dioxide during grinding in order to achieve edge-selective carboxylation (see Figure 1). Typically, the gas pressure of carbon dioxide, nitrogen and argon varied between 7 and 13 bar.

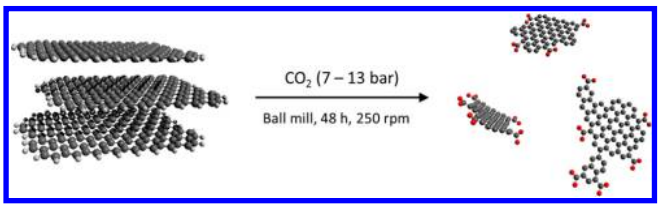

Figure 1. Edge-carboxylated graphene by dry grinding under CO_2 pressure.

In order to examine the role of metal abrasion, we used planetary ball mills with two different milling reactors and balls, both of which are made of either types of stainless steel or yttrium-stabilized zirconia ceramic. Typically, the milling reactor was charged with different amounts of dried graphite, evacuated to remove traces of oxygen and moisture, and then pressurized with oxygen-free dry carbon dioxide, nitrogen and argon. After grinding at 250 rpm for 48 h, the reactor was discharged under argon in order to prevent reaction with moisture and air. As observed by Jeon, when opening under air, violent sparkling occurred. The experimental results are summarized in Table 2, listing the elemental composition and metal content of the resulting nanocarbon materials, as measured by means of elemental analysis (EA) and energy-dispersive X-ray spectroscopy (EDX).

As it is apparent from Table 2, milling in the presence of carbon dioxide leads to high oxygen content up to around 17 wt %, mainly arising from the formation of carboxylic groups. The iron content is highly dependent on milling time, however the Fe-content in MG-CO_2-96-S is overestimated due to the combustion of carbon after violent sparkling when exposed to air. Under nitrogen pressure a mechanochemical nitrogen fixation of 5−8 wt % takes place, as previously reported by Jeon et al.[23] The resulting oxygen content of ∼10 wt % is due to oxidation when the milling reactor was opened in the presence of air. In contrast, ball milling of graphite under argon produced nonfunctionalized nanometer-scaled carbon in the absence of air. Obviously, highly reactive dangling bonds, formed during the milling process, are capable of reacting with carbon dioxide, nitrogen and also oxygen when carbon is exposed to air after milling.

The incorporation of functional groups was verified by means of IR spectroscopy. The FT-IR spectrum of the pristine graphite (Figure 2a) exhibits only a broad band at 3400 cm^{-1} and a weak signal at 1620 cm^{-1} indicating adsorbed water. The carboxylated MG-CO_2 shows the characteristic bands at 1710 cm^{-1} corresponding to the C═O stretching vibration, at 1585 cm^{-1} representing the CO_2^- asymmetric stretching vibration and at 1225 typical for the C−O−C mode. In addition, the products milled under argon and nitrogen (see Figure 2, traces b and c) showed C−H stretching vibration modes at 2920 and 2840 cm^{-1}. The peak at 1635 cm^{-1}, representing isolated C═C stretching modes, might be due to the extensive destruction of the aromatic π-system during the milling process.

Since all products were easily dispersible in most common solvents, TEM was used to analyze the particle morphology. After 12 h milling time the sheet like structure of the pristine graphite was partially maintained, as could be seen by the large and thin platelets. After 48 h of grinding, the particle size, as well as the platelet structure vanished. Only spherical nanoparticles were observed, as is apparent from the detailed enlargement, with average diameter of a few nanometers. Moreover, also the analysis of the AFM height profile confirmed that after prolonged grinding most nanoparticles exhibited cubic and spherical morphologies, whereas graphene-like flat structures were absent. Obviously, prolonged grinding affords high functionality at the expense of severe losses of the aspect ratio, as evidenced by the disappearance of the nanoplatelet structures especially after 96 h of milling. This is paralleled by an increase of the specific surface area from <10 m^2/g in graphite up to 350 m^2/g in MG-CO_2 as measured by the BET method.

Only when grinding was performed in stainless steel planetary ball mills in the presence of carbon dioxide and nitrogen, up to ∼30 wt % iron was detected after 96 h in the nanocarbon, whereas under argon and in ceramic ball mills no iron was incorporated. Yet, grinding with zirconia ball mills afforded only marginal amounts of zirconium impurities resulting from abrasion of the zirconia. While Jeon et al. carefully removed iron by treatment and washing with HCl[22] we used such iron "impurities" on nanocarbon to prepare carbon-supported iron catalysts for ethylene polymerization. It should be noted, that the electron microscopic investigation (see Figure 3) did not reveal the presence of iron nanoparticles. Therefore, we used Mössbauer spectroscopy to identify iron

dx.doi.org/10.1021/ma501602j | Macromolecules XXXX, XXX, XXX−XXX

Table 2. Elemental Composition of Milled Graphite (250 rpm, 48 h, 7−13 bar gas Pressure)

sample	gas	reactor	C[a] [wt %]	H[a] [wt %]	N[a] [wt %]	O[b] [wt %]	Fe[b] [wt %]	Zr[b] [wt %]
MG-CO_2-48-S	CO_2	steel	76.6	0.8	–	17.8	0.9	–
MG-CO_2-96-S[d]	CO_2	steel	27.8	0.9	–	27.6	29.1	–
MG-CO_2-48-C	CO_2	ceramic	79.2	0.8	–	17.3	–	0.8
MG-N_2-48-S	N_2	steel	83.0	0.5	8.1	11.5	0.3	–
MG-N_2-48-C	N_2	ceramic	79.7	0.3	5.3	10.4	–	2.2
MG-Ar-48-S	Ar	steel	87.8	0.4	0.4	–	1.1	–
MG-Ar-48-C	Ar	ceramic	88.8	–	–	10.2	–	0.8
graphite[c]	–	–	96.4	0.5	–	–	–	–

[a]From elemental analysis. [b]From EDX. [c]Pristine graphite prior to milling. [d]Violent sparkling after exposure to air; carbon combustion leads to underestimation of C-content and overestimation of Fe-content.

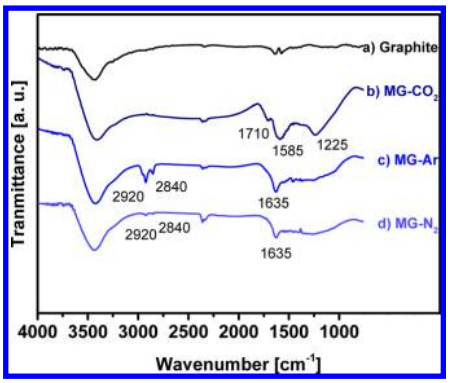

Figure 2. FT-IR spectra (KBr specimen) of the (a) pristine graphite, (b) MG-CO_2, (c) MG-Ar, and (d) MG-N_2.

and its oxidation state obtained after prolonged grinding of graphite.

According to Mössbauer spectroscopy, the Fe@MG-CO_2 sample, prepared by grinding under carbon dioxide pressure and stored under argon, contained predominantly Fe^{2+} together with Fe^0 (see Figure 4a). The characteristic new signal at chemical shift CS = 1.1 mm/s was only present if milled under carbon dioxide and disappeared if exposed to air. A chemical shift of CS > 1 mm/s is typical for ferrous sites, whereas the CS of ferric sites is well below 1 mm/s.[38] In contrast, grinding under nitrogen pressure produced iron-containing nitrogenated graphene, which does not stabilize Fe^{2+} by complexation. In fact, according to Figure 4b, Fe@MG-N2 contained predominantly Fe^0. Although more research is needed to clarify the mechanisms accounting for the Fe^{2+} formation on edge-carboxylated graphene, it is highly likely that electron transfer reactions occur either with radicals of graphene formed by prolonged grinding or with carboxyl radicals, formed by an addition mechanism as proposed by Jeon. However, the absence of any Fe^{2+} species in case of milling under nitrogen pressure indicates an electron transfer reaction only possible by the presence of MG-CO_2 in accord with observations by Jeon.[22] It is well-known, that carboxylates stabilize iron(II)[39] by complexation. However, when exposed to oxygen, ferrous sites readily oxidize to afford the corresponding ferric sites.

Using polymerization conditions as previously reported in more detail,[40] the Fe@MG-X were dispersed in *n*-heptane and activated by adding the bisiminopyridine (BIP) ligand, followed by activation with methylaluminoxane (MAO) after washing. Ethylene polymerization was carried out in *n*-heptane at 5 bar ethylene pressure and 40 °C, using an Al/Fe molar ratio of 100. The polymerization conditions and results are listed in Tables 1 and 3.

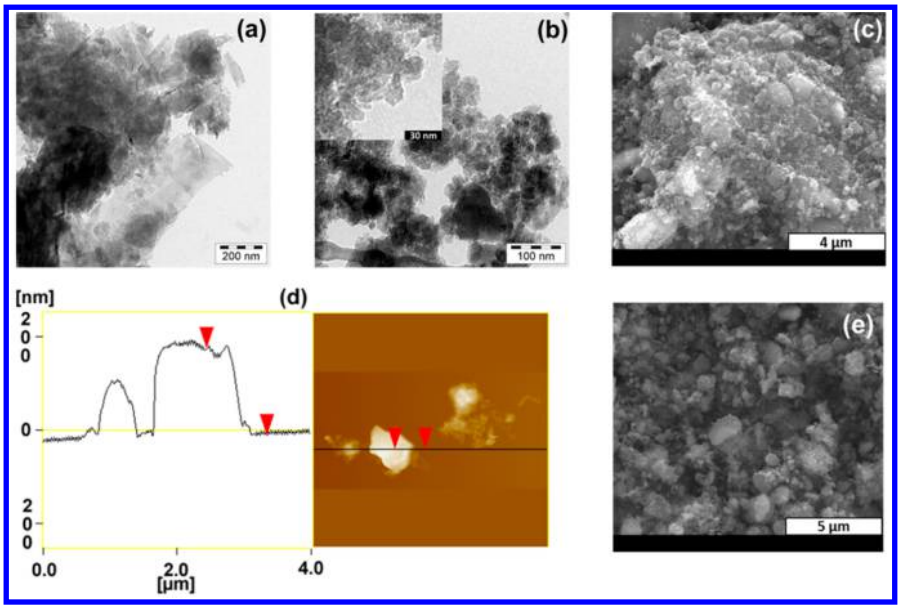

Figure 3. Micrographs of MG-CO_2: TEM images were taken from acetone dispersions: (a) ball milling for 12 h and (b) ball milling for 48 h. SEM image of a sample milled for 48 h (c) and 96 h (e). AFM measurement and height profile of MG-CO_2-48 h (d).

dx.doi.org/10.1021/ma501602j | Macromolecules XXXX, XXX, XXX−XXX

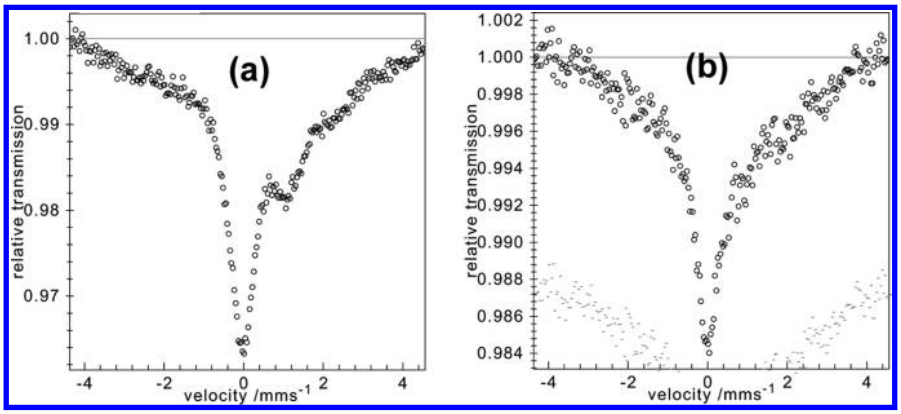

Figure 4. Fe–Mössbauer spectra recorded at 80 K of (a) Fe@MG-CO_2 stored under argon and (b) Fe@MG-N_2.

Table 3. Catalyst Composition and Polymer Properties

support Fe@MG-[b]	surface area [m^2/g]	n(Fe)[a] [μmol]	yield [g]	C-content [wt %]	molar mass (M_w) [kg/mol]	M_w/M_n	T_m [°C]
FeBIP	–	4.47	128	–	165	16	132
N_2-Ar	223	44.6	0	–	–	–	–
CO_2-atm	271	178	11.4	2.2	181	6.1	135
CO_2-Ar-48	273	44.6	30.5	0.8	177	8.3	134
CO_2-Ar-96 (0.2)	n.d.	250	117	0.2	283	6.1	136
CO_2-Ar-96 (5.0)[c]	n.d.	2500	49.4	5.0	80	6.3	131

[a]Sum of Fe^0, Fe^{II}, and Fe^{III} calculated by EDX measurement. [b]Polymerization parameters: m(support) = 250 mg, V_{pol} = 600 mL, t_{pol} = 120 min, Al/Fe = 100, p_{pol} = 5 bar, T_{pol} = 40 °C. [c]Yield-controlled polymerization for definite filler content; t_{Pol} = 10 min.

From Table 3 it is apparent that under the chosen conditions only the homogeneous catalyst FeBIP and the iron catalysts supported on edge-carboxylated graphene are active in ethylene polymerization, whereas Fe/C produced in the presence of nitrogen (Fe@MG-N_2) and argon are inactive. This is in accord with the results of the Mössbauer spectroscopic investigation, indicating the presence of Fe^{2+} exclusively in the case of Fe@MG-CO_2. It should be considered, that the Fe content given in Table 3 represents the sum of Fe^0, Fe^{II}, and Fe^{III} species. It was not possible to quantitatively determine the content of active Fe^{II} species, thus a relationship between Fe content and yield (molar mass) is not given at this point. From the polymerization kinetics displayed in Figure 5 it is apparent that exposure of Fe@MG-CO_2 to air, accompanied by massive oxidation of ferrous to ferric sites, drastically impairs catalysts activity. Interestingly, ethylene polymerization on Fe@MG-CO_2-Ar-96 produces the same amount of polyethylene as the polymerization with neat FeBIP. Figure 5 shows kinetics of the supported catalysts. It is obvious that milling graphite in a steel mill under CO_2 and storing it in the absence of oxygen under argon affords highly active catalysts. The performance of these catalysts leads to a yield that is in the same range as homogeneous MAO/FeBIP. The catalyst activities markedly increase with increasing milling time, showing that the grinding duration plays an important role. Milling under nitrogen or milling under argon or subsequent exposure to air drastically lowers polymerization activity. Obviously, oxidation of Fe^{2+} to Fe^{3+} significantly reduces the content of active sites. As is apparent from Table 3, the M_w of 181 kg/mol as well as the size distribution (PDI = 6.1) are in good agreement with the reported results of PE polymerizations realized with MAO/FeBIP and MAO-activated iron catalysts supported on silica.[40] Fe@MG-CO_2-96h (5.0) shows a lower molar mass which can be a result of the short polymerization time of 10 min. The excess of Fe in the reaction mixture attributed to a lower M_n (10 kg/mol) as a consequence of a higher number of catalytic centers. Since the Fe@MG-CO_2 catalysts contain substantial amounts of Fe^0, the resulting carbon/Fe/polyethylenes are magnetic. It should be noted that MG-CO_2–Ar-48, pretreated with MAO, can also be used as support for other single site catalysts such as $ZrCp_2Cl_2$.

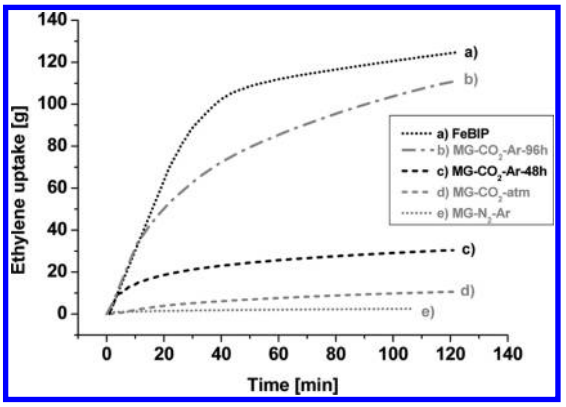

Figure 5. Online polymerization kinetics of ethylene polymerization on MAO-activated Fe@MG-X/BIP catalysts as compared to the homogeneous FeBIP/MAO catalysts; polymerization parameters: t_{Pol} = 10 min, Al/Fe = 100, p_{pol} = 5 bar, T_{pol} = 40 °C.

The carbon/polyethylene nanocomposites produced by ethylene polymerization on MAO/BIP-activated Fe@MG-CO_2 were melt processed by means of twin-screw mini-extrusion and subsequent micro injection molding. According to the transmission electron images (TEM) of PE containing 0.5 wt % Fe@MG-CO_2 (see Figure 6), the carbon particle diameter varies from a few nanometers to 500 nm in size. This is not surprising because the broad particle size distribution is identical to that of the milled carbon displayed in Figure 3,

dx.doi.org/10.1021/ma501602j | Macromolecules XXXX, XXX, XXX–XXX

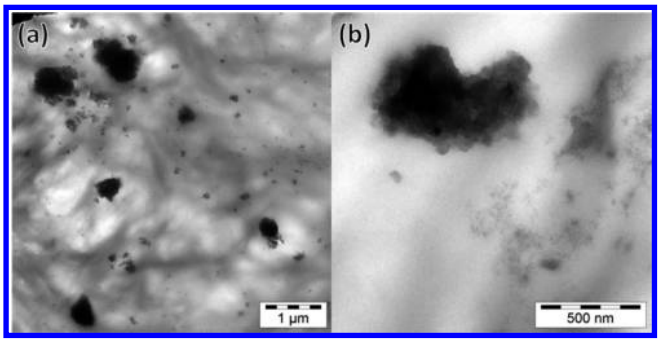

Figure 6. TEM images of a polyethylene containing 0.5 wt % Fe@MG-CO_2-48h.

parts c and e. Some agglomerates are present in the polymer composite. This is induced by the morphology of the pristine MG-CO_2 showing agglomerates and multilayered particles as a result of the milling process. The carbon/polyethylene nanocomposites were characterized by means of stress−strain measurements in order to determine their Young's modulus and elongation at break. Figure 7 compares the mechanical

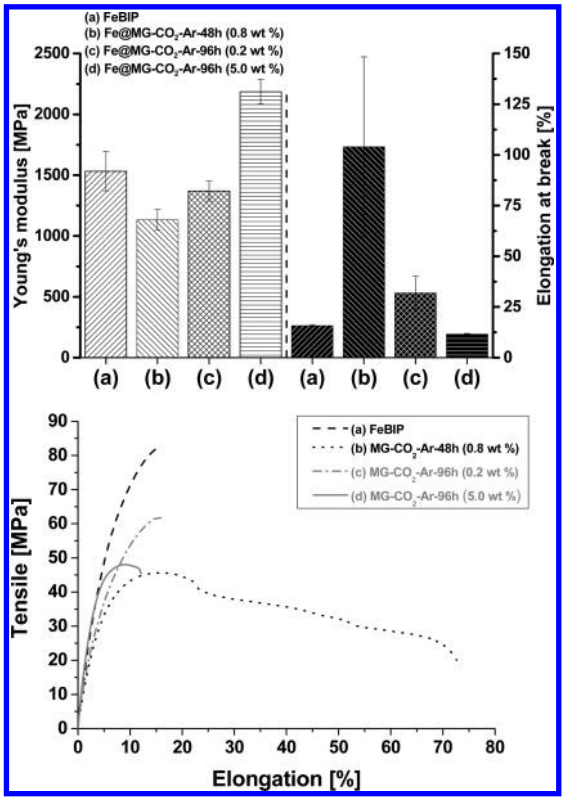

Figure 7. Young's modulus and elongation at break (left) of carbon/polyethylene composites (a) FeBIP, (b) Fe@MG-CO_2-Ar-48h (0.8 wt %), (c) Fe@MG-CO_2-Ar-96h (0.2 wt %), and (c) Fe@MG-CO_2-Ar-96h (5.0 wt %) and stress/strain−curves of the samples (right).

properties of the polyethylene produced by homogeneous FeBIP/MAO and by Fe@MG-CO_2/BIP/MAO polymerization, respectively. Obviously, the incorporation of Fe@MG-CO_2 accounts for markedly improved matrix reinforcement at carbon content of 5 wt % (Figure 7d). Thus, the mechanical properties are not related to the Fe content, instead the content of carbon based filler affect the mechanical properties. This is in good agreement with the performance of other graphene/polyolefin nanocomposites prepared by polymerization filling technique. Compared to graphene/polyethylene composites prepared by conventional melt compounding, elongation at break could be maintained, whereas Zheng et al reported on massive losses of elongation at break.[41]

CONCLUSION

We have developed a facile one-step mechanochemical process for the synthesis of iron polymerization catalysts supported on functionalized multilayer graphene for the preparation of carbon/polyolefin nanocomposites derived directly from graphite. Key feature is formation of an edge-carboxylated graphene as high-surface-area carbon support by chemical carbon dioxide fixation during grinding of graphite under carbon dioxide pressure. In this mechanochemical process, the formation of edge-selective carboxylated graphene is accompanied by the simultaneous immobilization of Fe^{2+}, resulting from abrasion of steel and electron transfer during milling. Unlike conventional graphene-supported polymerization catalysts, neither tedious multistep catalyst preparation nor the use of graphite oxide as intermediate is required. Ethylene polymerization takes place when Fe@MG-CO_2 is activated by the subsequent addition of BIP and MAO. According to Mössbauer spectroscopy, the presence of Fe^{2+} is crucial for achieving activity in ethylene polymerization. When Fe@MG-CO_2 is exposed to air, ferrous sites are converted into inactive ferric sites, thus accounting for drastically lowering catalyst activities. Polymerization activity increases with increasing milling time, which is paralleled by increasing the amount of immobilized iron and carboxylate groups. Further investigations showed, that the overall Fe content is reliably controllable by milling time and CO_2 pressure. This mechanochemical process for producing nanocarbon-supported iron catalysts is an attractive route to carbon/polyolefin nanocomposites prepared by the polymerization filling technique. Owing to the drastic reduction of graphene aspect ratio during prolonged grinding, the matrix reinforcement of such edge-carboxylated graphene is considerably lower with respect to that of graphene/polyolefin nanocomposites based upon thermally reduced graphite oxide. However, this mechanochemical route to carbon/polyolefin compounds is cost-effective and enables the incorporation of much larger carbon nanoparticle content without impairing processing. This offers new opportunities for designing carbon/polyolefin composite materials with high electrical and thermal conductivity for potential applications in lightweight engineering.

AUTHOR INFORMATION

Corresponding Author

*(R.M.) E-mail: rolf.muelhaupt@makro.uni-freiburg.de.

Author Contributions

[§]Authors contributed equally.

Notes

The authors declare no competing financial interest.

ACKNOWLEDGMENTS

The authors gratefully acknowledge the financial support by the European Commission within the Graphene Flagship (GAN 604391). The authors thank A. Warmbold and J. Eckerle for their support doing the experimental work.

REFERENCES

(1) Novoselov, K. S.; Geim, A. K.; Morozov, S. V.; Jiang, D.; Zhang, Y.; Dubonos, S. V.; Grigorieva, I. V.; Firsov, A. A. *Science* **2004**, *306*, 666.
(2) Lee, C.; Wei, X.; Kysar, J. W.; Hone, J. *Science* **2008**, *321*, 385.
(3) Kim, K. S.; Zhao, Y.; Jang, H.; Lee, S. Y.; Kim, J. M.; Kim, K. S.; Ahn, J.-H.; Kim, P.; Choi, J.-Y.; Hong, B. H. *Nature* **2009**, *457*, 706.
(4) Cranford, S. W.; Buehler, M. J. *Phys. Rev. B* **2011**, *84*, 205451.
(5) Scheuermann, G. M.; Rumi, L.; Steurer, P.; Bannwarth, W.; Mülhaupt, R. *J. Am. Chem. Soc.* **2009**, *131*, 8262.
(6) Wan, Q.; Liu, Y.; Wang, Z.; Wei, W.; Li, B.; Zou, J.; Yang, N. *Electrochem. Commun.* **2013**, *29*, 29.
(7) Stürzel, M.; Kempe, F.; Thomann, Y.; Mark, S.; Enders, M.; Mülhaupt, R. *Macromolecules* **2012**, *45*, 6878−6887.
(8) Lim, D.-H.; Wilcox, J. *J. Phys. Chem. C* **2012**, *116*, 3653.
(9) Gomez De Arco, L.; Zhang, Y.; Schlenker, C. W.; Ryu, K.; Thompson, M. E.; Zhou, C. *ACS Nano* **2010**, *4*, 2865.
(10) Wang, X.; You, H.; Liu, F.; Li, M.; Wan, L.; Li, S.; Li, Q.; Xu, Y.; Tian, R.; Yu, Z.; Xiang, D.; Cheng, J. *Chem. Vap. Deposition* **2009**, *15*, 53.
(11) Avouris, P.; Dimitrakopoulos, C. *Mater. Today* **2012**, *15*, 86.
(12) Mauro, M.; Cipolletti, V.; Galimberti, M.; Longo, P.; Guerra, G. *J. Phys. Chem. C* **2012**, *116*, 24809.
(13) Tölle, F. J.; Fabritius, M.; Mülhaupt, R. *Adv. Funct. Mater.* **2012**, *22*, 1136.
(14) Brodie, B. C. *Philos. Trans. R. Soc. London* **1859**, *149*, 249.
(15) Hummers, W. S.; Offeman, R. E. *J. Am. Chem. Soc.* **1958**, *80*, 1339.
(16) Stankovich, S.; Dikin, D. A.; Piner, R. D.; Kohlhaas, K. A.; Kleinhammes, A.; Jia, Y.; Wu, Y.; Nguyen, S. T.; Ruoff, R. S. *Carbon* **2007**, *45*, 1558.
(17) Eda, G.; Fanchini, G.; Chhowalla, M. *Nat. Nanotechnol.* **2008**, *3*, 270.
(18) Knieke, C.; Berger, A.; Voigt, M.; Taylor, R. N. K.; Röhrl, J.; Peukert, W. *Carbon* **2010**, *48*, 3196.
(19) Zhao, W.; Fang, M.; Wu, F.; Wu, H.; Wang, L.; Chen, G. *J. Mater. Chem.* **2010**, *20*, 5817.
(20) Wu, H.; Zhao, W.; Chen, G. *J. Appl. Polym. Sci.* **2011**, *125*, 3899.
(21) Leon, V.; Quintana, M.; Herrero, M. A.; Fierro, J. L. G.; Hoz, A. d. l.; Prato, M.; Vazquez, E. *Chem. Commun.* **2011**, *47*, 10936.
(22) Jeon, I.-Y.; Shin, Y.-R.; Sohn, G.-J.; Choi, H.-J.; Bae, S.-Y.; Mahmood, J.; Jung, S.-M.; Seo, J.-M.; Kim, M.-J.; Wook Chang, D.; Dai, L.; Baek, J.-B. *Proc. Natl. Acad. Sci. U. S. A.* **2012**, *109*, 5588.
(23) Jeon, I.-Y.; Choi, H.-J.; Ju, M. J.; Choi, I. T.; Lim, K.; Ko, J.; Kim, H. K.; Kim, J. C.; Lee, J.-J.; Shin, D.; Jung, S.-M.; Seo, J.-M.; Kim, M.-J.; Park, N.; Dai, L.; Baek, J.-B. *Sci. Rep.* **2013**, *3*, 2260.
(24) Lee Jae Kap, L. Kyoung-Il, *Vol.* US2012043402 (A1), K. I. S. Tech.:Korea, 2010.
(25) Welham, N. J.; Williams, J. S. *Carbon* **1998**, *36*, 1309.
(26) Anna, M.; Albert, G. N.; Esko, I. K. *J. Phys.: Condens. Matter* **2003**, *15*, S3011.
(27) Sun, C.-L.; Li, B.-J.; Shi, Z.-J. *Chem. Rev.* **2010**, *111*, 1293.
(28) Dry, M. E. *Catal. Today* **2002**, *71*, 227.
(29) Lane, B. S.; Burgess, K. *Chem. Rev.* **2003**, *103*, 2457.
(30) Britovsek, G. J. P.; Bruce, M.; Gibson, V. C.; Kimberley, B. S.; Maddox, P. J.; Mastroianni, S.; McTavish, S. J.; Redshaw, C.; Solan, G. A.; Stromberg, S.; White, A. J. P.; Williams, D. J. *J. Am. Chem. Soc.* **1999**, *121*, 8728.
(31) Janiak, C.; Rieger, B. *Angew. Makromol. Chem.* **1994**, *215*, 47.
(32) Schilling, M.; Bal, R.; Görl, C.; Alt, H. G. *Polymer* **2007**, *48*, 7461.
(33) Schmidt, R.; Welch, M. B.; Palackal, S. J.; Alt, H. G. *J. Mol. Catal. A: Chem.* **2002**, *179*, 155.
(34) Small, B. L.; Brookhart, M. *J. Am. Chem. Soc.* **1998**, *120*, 7143.
(35) Alexandre, M.; Dubois, P.; Sun, T.; Garces, J. M.; Jerôme, R. *Polymer* **2002**, *43*, 2123.
(36) Quan, Y. N.; Lu, M.; Tian, M.; Yan, S. K.; Yu, Z. Z.; Zhang, L. Q. *J. Appl. Polym. Sci.* **2013**, *130*, 680.
(37) Fim, F. D.; Basso, N. R. S.; Graebin, A. P.; Azambuja, D. S.; Galland, G. B. *J. Appl. Polym. Sci.* **2013**, *128*, 2630.
(38) Williams, A. G. B.; Scherer, M. M. *Environ. Sci. Technol.* **2004**, *38*, 4782.
(39) Lippard, S. J. *Philos. Trans. R. Soc. A: Math., Phys. Eng. Sci.* **2005**, *363*, 861.
(40) Kurek, A.; Mark, S.; Enders, M.; Kristen, M. O.; Mülhaupt, R. *Macromol. Rapid Commun.* **2010**, *31*, 1359.
(41) Zheng, W.; Lu, X.; Wong, S.-C. *J. Appl. Polym. Sci.* **2004**, *91*, 2781.